

# Molding topologically-complex 3D polymer microstructures from femtosecond laser machined glass

Allison Schaap and Yves Bellouard\*

Department of Mechanical Engineering, Eindhoven University of Technology, Postbus 513, 5600MB Eindhoven, The Netherlands

Fax: + 31-40-247-2603; Tel: + 31-40-247-3715

\*y.bellouard@tue.nl, a.schaap@tue.nl

**Abstract:** The fabrication of complex, three-dimensional microscale shapes that can be replicated over large surfaces is an ongoing challenge, albeit one with a wide range of possible applications such as engineered surfaces with tuned wetting properties, scaffolds for cell studies, or surfaces with tailored optical properties. In this work, we use a two-step femtosecond laser direct-write technique and wet-etching process to fabricate monolithic glass micromolds with complex three-dimensional surface topologies, and demonstrate the replication of these structures in a soft polymer (polydimethylsiloxane, PDMS). To estimate the forces experienced during the demolding for one representative structure, we use a combination of two models – a simple linear elastic model and a numerical hyperelastic model. These models are used to support the high experimental success rates of the demolding process observed, despite the high strain induced in the material during demolding. Since the process used is scalable, this work opens new avenues for low-cost fabrication of surfaces having complex microscale patterns with three-dimensional geometries.

©2013 Optical Society of America

**OCIS codes:** (220.4000) Microstructure fabrication; (220.4610) Optical fabrication; (140.3390) Laser materials processing; (140.7090) Ultrafast lasers; (160.2750); Glass and other amorphous materials; (160.5470) Polymers.

---

## References and links

1. A. Jagota and C.-Y. Hui, "Adhesion, friction, and compliance of bio-mimetic and bio-inspired structured interfaces," *Mater. Sci. Eng. R-Reports* **72**, 253–292 (2011).
2. Y. Bellouard, A. Said, M. Dugan, and P. Bado, "Fabrication of high-aspect ratio, micro-fluidic channels and tunnels using femtosecond laser pulses and chemical etching," *Opt. Express* **12**(10), 2120–2129 (2004).
3. D. Sameoto and C. Menon, "A low-cost, high-yield fabrication method for producing optimized biomimetic dry adhesives," *J. Micromech. Microeng.* **19**(11), 115002 (2009).
4. T. G. Leong, A. M. Zarafshar, and D. H. Gracias, "Three-dimensional fabrication at small size scales," *Small* **6**(7), 792–806 (2010).
5. J. G. Fernandez and A. Khademhosseini, "Micro-masonry: Construction of 3D structures by microscale self-assembly," *Adv. Mater.* **22**(23), 2538–2541 (2010).
6. N. Bassik, G. M. Stern, M. Jamal, and D. H. Gracias, "Patterning thin film mechanical properties to drive assembly of complex 3D structures," *Adv. Mater.* **20**(24), 4760–4764 (2008).
7. C. Py, P. Reverdy, L. Doppler, J. Bico, B. Roman, and C. N. Baroud, "Capillary Origami: Spontaneous Wrapping of a Droplet with an Elastic Sheet," *Phys. Rev. Lett.* **98**(15), 156103 (2007).
8. S. Maruo and J. T. Fourkas, "Recent progress in multiphoton microfabrication," *Laser Photonics Rev.* **2**(1-2), 100–111 (2008).
9. Y.-L. Zhang, Q.-D. Chen, H. Xia, and H.-B. Sun, "Designable 3D nanofabrication by femtosecond laser direct writing," *Nano Today* **5**(5), 435–448 (2010).
10. D. Kim and P. T. C. So, "High-throughput three-dimensional lithographic microfabrication," *Opt. Lett.* **35**(10), 1602–1604 (2010).
11. C. Acikgoz, M. A. Hempenius, J. Huskens, and G. J. Vancso, "Polymers in conventional and alternative lithography for the fabrication of nanostructures," *Eur. Polym. J.* **47**(11), 2033–2052 (2011).

12. C. N. LaFratta, T. Baldacchini, R. A. Farrer, J. T. Fourkas, M. C. Teich, B. E. A. Saleh, and M. J. Naughton, "Replication of two-photon-polymerized structures with extremely high aspect ratios and large overhangs," *J. Phys. Chem. B* **108**(31), 11256–11258 (2004).
13. S. Maruo, "Femtosecond laser stereolithography and replication technique for MEMS application," in *Conference on Lasers Electro Optics The Pacific Rim Conference on Lasers and Electro-Optics, 2009. CLEO/PACIFIC RIM '09* (2009), pp. 1–2.
14. D. Sameoto and C. Menon, "Recent advances in the fabrication and adhesion testing of biomimetic dry adhesives," *Smart Mater. Struct.* **19**(10), 103001 (2010).
15. L. F. Boesel, C. Greiner, E. Arzt, and A. del Campo, "Gecko-inspired surfaces: A path to strong and reversible dry adhesives," *Adv. Mater.* **22**(19), 2125–2137 (2010).
16. C. Greiner, A. D. Campo, and E. Arzt, "Adhesion of bioinspired micropatterned Surfaces: Effects of pillar radius, aspect ratio, and preload," *Langmuir* **23**(7), 3495–3502 (2007).
17. F. Madani-Grasset and Y. Bellouard, "Femtosecond laser micromachining of fused silica molds," *Opt. Express* **18**(21), 21826–21840 (2010).
18. K. M. Choi and J. A. Rogers, "A photocurable poly(dimethylsiloxane) chemistry designed for soft lithographic molding and printing in the nanometer regime," *J. Am. Chem. Soc.* **125**(14), 4060–4061 (2003).
19. X. Q. Brown, K. Ookawa, and J. Y. Wong, "Evaluation of polydimethylsiloxane scaffolds with physiologically-relevant elastic moduli: interplay of substrate mechanics and surface chemistry effects on vascular smooth muscle cell response," *Biomaterials* **26**(16), 3123–3129 (2005).
20. F. Schneider, T. Fellner, J. Wilde, and U. Wallrabe, "Mechanical properties of silicones for MEMS," *J. Micromech. Microeng.* **18**(6), 065008 (2008).
21. D. Fuard, T. Tzvetkova-Chevolleau, S. Decossas, P. Tracqui, and P. Schiavone, "Optimization of poly-dimethyl-siloxane (PDMS) substrates for studying cellular adhesion and motility," *Microelectron. Eng.* **85**(5-6), 1289–1293 (2008).
22. R. N. Palchesko, L. Zhang, Y. Sun, and A. W. Feinberg, "Development of Polydimethylsiloxane Substrates with Tunable Elastic Modulus to Study Cell Mechanobiology in Muscle and Nerve," *PLoS ONE* **7**(12), e51499 (2012).
23. M. Liu, J. Sun, Y. Sun, C. Bock, and Q. Chen, "Thickness-dependent mechanical properties of polydimethylsiloxane membranes," *J. Micromechanics Microengineering* **19**, 035028 (2009).
24. T. K. Kim, J. K. Kim, and O. C. Jeong, "Measurement of nonlinear mechanical properties of PDMS elastomer," *Microelectron. Eng.* **88**(8), 1982–1985 (2011).
25. D. P. J. Cotton, A. Popel, I. M. Graz, and S. P. Lacour, "Photopatterning the mechanical properties of polydimethylsiloxane films," *J. Appl. Phys.* **109**(5), 054905 (2011).
26. A. Mata, A. J. Fleischman, and S. Roy, "Characterization of polydimethylsiloxane (PDMS) properties for biomedical micro/nanosystems," *Biomed. Microdevices* **7**(4), 281–293 (2005).
27. J. Flueckiger, V. Bazargan, B. Stoeber, and K. C. Cheung, "Characterization of postfabricated parylene C coatings inside PDMS microdevices," *Sens. Actuators B Chem.* **160**(1), 864–874 (2011).
28. S. Rajesh and Y. Bellouard, "Towards fast femtosecond laser micromachining of fused silica: The effect of deposited energy," *Opt. Express* **18**(20), 21490–21497 (2010).
29. S. Juodkazis, K. Yamasaki, V. Mizeikis, S. Matsuo, and H. Misawa, "Formation of embedded patterns in glasses using femtosecond irradiation," *Appl. Phys. Mater. Sci. Process.* **79**(4-6), 1549–1553 (2004).
30. S. Kiyama, S. Matsuo, S. Hashimoto, and Y. Morihira, "Examination of etching agent and etching mechanism on femtosecond laser microfabrication of channels inside vitreous silica substrates," *J. Phys. Chem. C* **113**(27), 11560–11566 (2009).
31. Y. Bellouard, A. Champion, B. Lensen, M. Matteucci, A. Schaap, M. Beresna, C. Corbari, M. Gecevicius, P. Kazansky, O. Chappuis, M. Kral, R. Clavel, F. Barrot, J.-M. Breguet, Y. Mabillard, S. Bottinelli, M. Hopper, C. Hoenninger, E. Mottay, and J. Lopez, "The femto-print project," *J. Laser Micronanoengineering* **7**(1), 1–10 (2012).

---

## 1. Introduction

The design and abilities of microscale devices are often limited by the fabrication processes available. For lab on a chip devices, most common fabrication processes have inherent two-dimensionality, or limited three-dimensionality. However, the creation of three-dimensional features for microdevices has many applications, including surfaces with engineered wetting, adhesion and optical properties [1]. Here, we present an enabling technology that allows the fabrication of truly user-definable three-dimensional microfeatures on glass surfaces. As shown in Fig. 1, we use a femtosecond laser to locally modify (but not ablate) glass with a multi-photon absorption process [2]. The modification process is non-linear: only regions in which the laser power exceeds a threshold value are affected. As a result, truly three-dimensional patterns can be created, without modifying the material outside of the laser focal volume. The laser-modified glass regions are susceptible to a chemical etch at a rate much

faster than that of the pristine material, which allows the exposed regions to be removed selectively, creating structures as defined by the laser exposure pattern. After exposure and etching, a negative of the resulting substrate is replicated with the silicone polydimethylsiloxane (PDMS). This molding process results in a monolithic material with completely custom-patterned three-dimensional surface features, for example those in Fig. 1 (bottom).

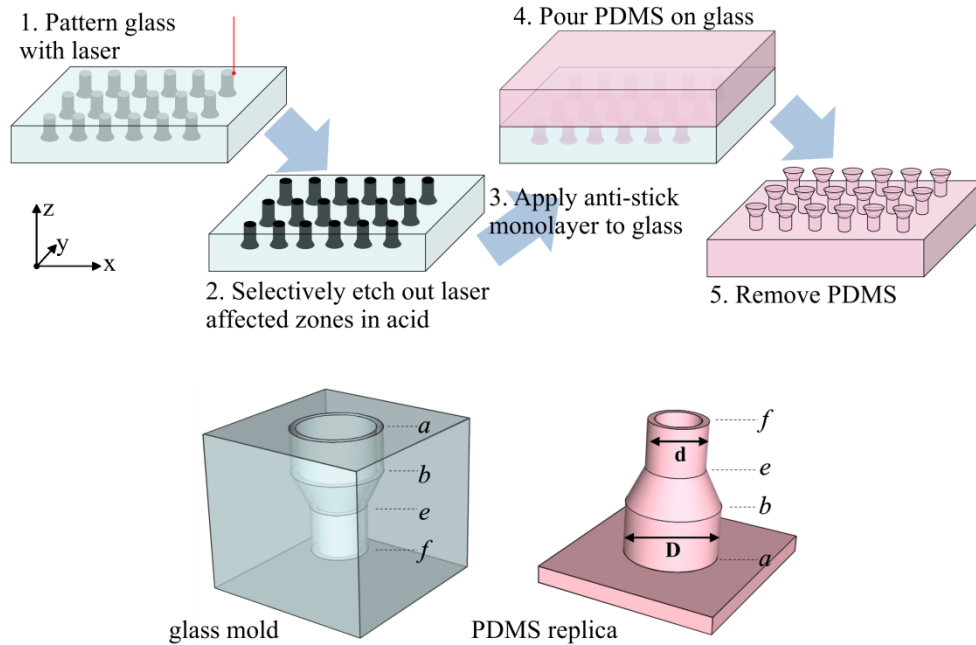


Fig. 1. (Top) Fabrication process: a femtosecond laser modifies regions of the fused silica substrate (step 1); the modified regions are selectively etching 2.5% hydrofluoric acid (step 2); after the application of a chemical treatment to decrease mold adhesion (step 3), PDMS is poured over the glass mold (step 4), cured, and removed (step 5). (Bottom) The test structure; thin-shelled cylinders of varying diameter were fabricated, with the nominal (machined) ratios of  $1/3 \leq d/D \leq 3$ . Each section is  $75 \mu\text{m}$  high, and the largest diameter is  $100 \mu\text{m}$ ; the diameter of the other sections are varied to change the  $d/D$  ratio.

Most existing standard microfabrication processes offer limited inherent three-dimensionality. Mask-based photolithography processes in particular are primarily restricted to multiple two-dimensional layers, or to forming structures of limited three-dimensionality through undercutting [3] or greyscale lithography. Additionally, features in the third dimension can be formed post-lithography through self-assembling mechanisms [4,5] using for example thin-film stresses [6] or capillary forces [7]. Alternative approaches such as 2-photon polymerization [8–10] and electron-beam lithography [11] have been demonstrated, but are slow to process, and still serial in nature. To overcome the intrinsic throughput limit of these processes, polymer structures fabricated by two-photon lithography have also been used as molds [12,13], although polymer molds can withstand restricted thermal and mechanical stresses.

The technique presented here, on the other hand, offers many advantages. First, the laser-write process means that the machinable surface area is limited only by the size of the substrate or the range of motion of the stages used to manipulate it with respect to the laser beam. Second, the resulting mold is made of a single strong, transparent, and inert material and is thus suitable for numerous low-cost replications without concerns for mold degradation (such as material delamination for multi-layer molds). Additionally, the complexity of the designed shapes has no direct influence on the fabrication process: the process remains two-

step - laser direct-write followed by etching - regardless of the final pattern complexity. The formation of complex geometries simply requires the appropriate programming of the stages used in the laser exposure.

In this paper, we use PDMS as a test molding material to create negative replicas of the laser-machined glass, as PDMS can withstand large strains, is already commonly used in microfluidic and micromolding applications [14–16], and is optically transparent, which could be advantageous in applications involving, for example, the microscopy of organisms or cells inside of the fabricated microstructures. We have previously demonstrated the demolding of pillars and microchannels fabricated with femtosecond laser machining, particularly as a tool for studying the geometry and machining quality of the structures [17].

Here, we systematically study the capabilities and limitations of this molding process as a fabrication technique. We present a wide variety of complex 3D microstructures, primarily thin-walled hollow vessels. One shape in particular, shown in Fig. 1 (bottom), is studied in detail analytically, numerically, and experimentally. This one was chosen in particular because it serves as an illustrative, non-trivial example of the process: the PDMS must withstand large tensile strains to undergo successful demolding. The radial symmetry of the shape allows for both analytical and numerical evaluation of the stresses, which are then compared to the results of the demolding process. The molding process has a high rate of success, even for shapes which impose significant strain in the PDMS during demolding.

## 2. Fabrication and methodology

An overview of the fabrication process is shown in Fig. 1. The patterns were defined with a ytterbium-fiber based laser (1030 nm) with pulse duration of approximately 350 fs; the repetition rate of the laser was 400 kHz and the average energy 220 mW, yielding a pulse energy of 550 nJ/pulse. The glass (fused silica) sample was affixed to stages moving at a speed of 2 mm/s in the two directions perpendicular to the beam axis (x and y axes in Fig. 1). The position of the laser focal point along the z axis was controlled by moving the 20x objective lens (NA = 0.4) with a third stage. The exposure of test shapes as shown in Fig. 1 was accomplished by exposing subsequent circles on the x-y plane with a z-offset between layers of 5  $\mu\text{m}$  for the cylindrical sections (e.g. sections a-b, e-f, Fig. 1), and 2.5  $\mu\text{m}$  for the conical sections (e.g. section b-e, Fig. 1).

Following exposure, the sample was etched in 2.5% hydrofluoric acid (HF) at room temperature for 9.5 hours. After the etching is complete, the samples were coated with a nanometers-thick monolayer of high-density PDMS to decrease the adhesion between the glass and the polymer. The process is described in detail in previous work [17]; in short, this monolayer was made with silanol-terminated PDMS macromolecules with an average molecular weight of 139 kg/mol (Gelest, Inc). It is prepared in an octane solvent at 50% v/v, deposited on the mold, allowed to evaporate, incubated, and the excess monomer rinsed off with toluene. The monomers bind to the fused silica during the incubation step and, upon final exposure to air, collapse onto the substrate where they decrease the adhesion between the glass and the two-part PDMS later used to replicate the structures.

For mold replication, PDMS (Sylgard 184) was mixed in a 1:10 ratio of hardener:base, poured on the mold, cured at 65°C for 2 hours, and allowed to return to room temperature over several hours. The glass mold and polymer replica were then separated by hand, and the PDMS was coated with gold (approx. 70 nm thick) for SEM imaging of the structures.

## 3. Modeling of the structures

There are significant uncertainties in modeling the demolding behavior of PDMS: values in the literature for PDMS mechanical properties are varied, the strain rate at which we demold the devices is unknown, and quantitative data on the decrease in coefficient of friction between the treated glass and the PDMS is not available. However, we compare two simple models to predict the approximate values of  $d/D$  for which the demolding process is likely to

be successful, and to examine the qualitative effects of the various unknowns on the demolding process.

#### *Analytical model: PDMS as a linear elastic material*

Our first model treats PDMS as a linearly elastic material and estimates the combined stresses from the hoop-wise stretching of the PDMS and the friction during demolding. The most prevalent type of PDMS used in microfabrication is Sylgard 184 (Dow Corning) mixed at a 1:10 ratio, and all further material property values in this paper are specific to this formulation unless otherwise mentioned.

#### *PDMS material properties*

While the stress-strain curve of PDMS is non-linear for large strains, the region with strain less than 0.4 can be approximated as linear. The most commonly-reported value of the elastic modulus of bulk PDMS in this region is around 1.8 MPa [18–22]. However, the measured values of the elastic modulus depend on the curing process and on the thickness of the PDMS. For example, values of between 0.8 MPa and 4 MPa were found for samples prepared with significantly shorter and longer than recommended curing times, respectively [21]. Additionally, a transition from bulk to thickness-dependent elasticity has been reported at a film thickness of around 200  $\mu\text{m}$  [23]; the elastic modulus measured in a 50  $\mu\text{m}$  thin film was roughly twice that of a 1 mm thick sample. The variance in reported values also seems to increase with decreasing thickness: the elastic modulus of samples of thickness around 100  $\mu\text{m}$  has been reported from 0.3 MPa [24] to 2.9 MPa [25], with little agreement between studies.

The ultimate tensile strength (UTS) of bulk PDMS is reported at 7.5 MPa [26], but has been shown to increase dramatically with thinner membranes. A UTS of 100 MPa was reported for a 30  $\mu\text{m}$  thick membrane, compared to 20 MPa measured on membranes of thicknesses in the hundreds of microns [23]. Our devices have wall thicknesses of 8-9  $\mu\text{m}$  in the region between marks *e* and *f* in Fig. 1 (bottom).

#### *Effects of machined deviations from design*

After etching, the geometry of the holes is not exactly as originally written, so the final geometry of the structures was measured and used as input to the model. The geometry of the final shapes is affected by two parameters considered here: the laser focal volume shape and the non-zero etching rate of the pristine material in the acid. The laser focal volume has a finite width, and modified a region of material with an in-plane diameter of about 3  $\mu\text{m}$ , as measured on the surface of the material after exposure. The pristine material – that unaffected by the femtosecond laser – is also etched by the hydrofluoric acid, although at a much lower rate than the exposed regions. Based on measurements through the side of the glass during the etching process, the axial etching rate (into the depth of the material along the etched patterns) was estimated at  $29 \pm 2 \mu\text{m/hr}$  on average. From measurements of the size of the patterns on the surface, the in-plane etch rate of the pristine material was estimated at  $0.78 \pm 0.02 \mu\text{m/hr}$ . SEM images of the demolded PDMS show that the wall thickness at the top of the PDMS is 8.6  $\mu\text{m}$ . These values were used to estimate the diameter of the inner glass core of the molds and the wall thickness of the PDMS mold between the top and bottom of the structures.

#### *Stress calculations for linear material assumption*

To predict the success of the demolding of structures such as those shown in Fig. 1 and Fig. 3(a), we model a combined load on the structure at the point of highest stress, when the narrowest-diameter section of the PDMS (the section between *e* and *f*, Fig. 1) is stretched around the widest-diameter section of the glass (the section between points *a* and *b*, Fig. 1). The loading is a combination two forces. First, there is the hoop force

$$F_{hoop} = \epsilon EtL \quad (1)$$

where  $\epsilon$  is the strain created by stretching the PDMS of diameter  $d$  around the larger glass cylinder of diameter  $D$ ,  $E$  is the elastic modulus,  $t$  is the PDMS wall thickness, and  $L$  is the length of the section ( $75 \mu\text{m}$ ). Second, the friction force opposing the demolding is estimated by

$$F_{friction} = \mu \epsilon EA \quad (2)$$

with  $\mu$  the coefficient of friction, and  $A$  the surface area in contact.

The two forces are combined and compared to the ultimate tensile strength of PDMS by the von Mises criterion.

#### *Numerical modeling: PDMS as a hyperelastic material*

Since PDMS has a non-linear stress-strain curve, the use of the linear elastic model above introduces errors in the estimation of the stresses induced by the demolding process. To estimate these errors, we use two hyperelastic material models implemented in COMSOL Multiphysics, and use the results to estimate uncertainties for the analytical model.

First, we model the simple radial expansion of a thin-walled cylinder of hyperelastic PDMS and compare the results of this COMSOL model to those of the hoop stress calculated with the linear elastic analytical model. While this numerical model does not capture the full forces exerted on the PDMS during demolding – it ignores the axial strain from the demolding, as well as the friction and adhesion forces at the PDMS-glass interface – it offers a first quantification of the errors introduced by using the linear elastic material model. In this first hyperelastic model, shown in Fig. 2(a), the PDMS is initially sitting around a cylinder of a material with an extremely low Young's modulus and Poisson's ratio. The line at the interface of the two materials is moved radially outwards a fixed distance, and the maximum von Mises stress in the PDMS as a function of the distance is obtained.

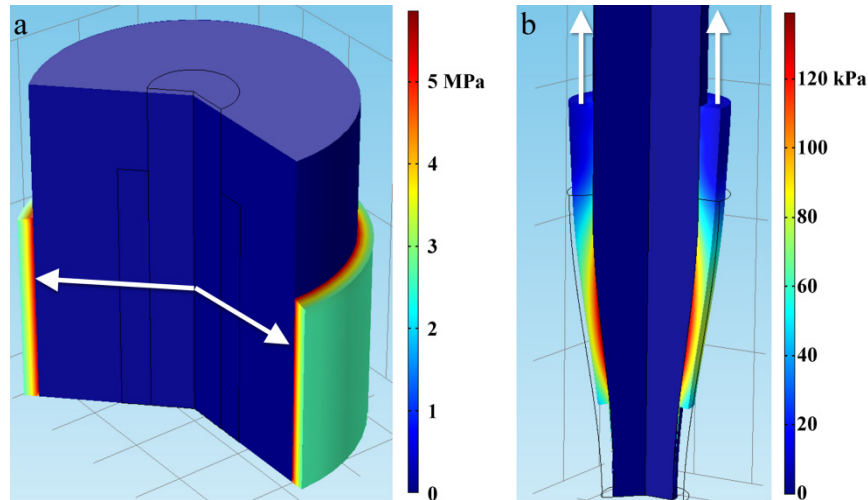


Fig. 2. The COMSOL model used to determine the maximum von Mises stresses on the PDMS using the Mooney-Rivlin hyperelastic material formulation. The first model (a) merely imposed a radial expansion on the PDMS for every combination of  $d/D$  values tested experimentally. The second model (b) modeled the complete geometry and demolding process for the middle  $d/D$  ratio. In both models, the direction of motion in the model is indicated with white arrows, and the instantaneous von Mises stress on the PDMS is plotted.

The second model (Fig. 2(b)) uses a two-material system which mimics as closely as possible the physical demolding process, with forces imposed in both the radial and axial

directions. The hyperelastic PDMS starts in an initial stress-free state and is removed from the fixed inner glass core with a constant velocity. The profile of the contact line between the glass and the PDMS is defined with cubic Bezier curves to prevent areas of high discontinuities, and the height of the inner glass core is increased to avoid discontinuities at the surface of the glass. A two-parameter Mooney-Rivlin formulation is used to model the hyperelastic behavior of the PDMS. The Mooney-Rivlin model uses two constants ( $C_{10}$  and  $C_{01}$ ) to characterize the material; much like the range of elastic moduli found in the literature, the range of constants reported for PDMS vary. Of three reports of Mooney-Rivlin models of Sylgard 184 with a ratio of 1:10, two have  $C_{01}$  at zero, reducing the model to a neo-Hookean solid. The value of  $C_{10}$  ranges from 70.5 kPa [24] to 321 kPa [25], with a change in this value from 205 kPa to 321 kPa reported as a result of an increase in PDMS bake time [25]. In our model, the hyperelastic constant  $C_{10}$  is varied to evaluate its effect on the stress estimates.

## Results

Figure 3 shows examples of some of the demolded structures; only the case shown in 3a ( $d/D < 1$ ) is modeled. The data from the model and the successful demolding rates for this shape are shown in Fig. 4. Fifteen different values of  $d/D$  were used; each one was repeated 25 times at different locations spread across on the substrate, creating a total of 375 samples. The samples with  $d/D < 1$  made up 175 of these.

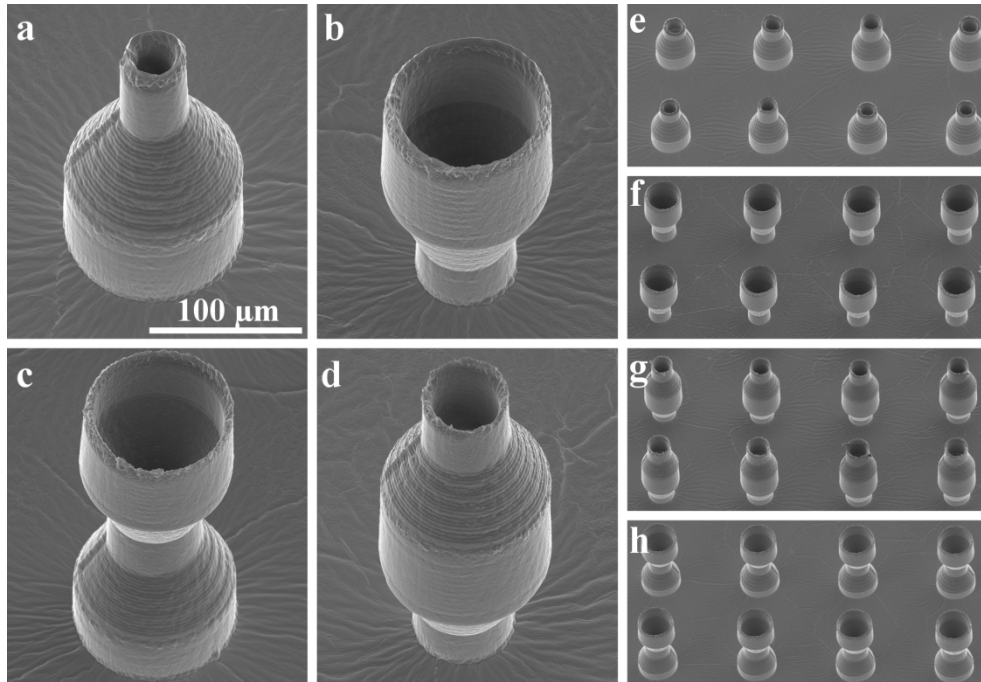


Fig. 3. SEM images of the PDMS mold, after being demolded from the glass and coated with gold for imaging. Single (a, b) and double (c, d) shapes are shown, with  $d/D < 1$  (a) and  $d/D > 1$  (b). The shapes as in (a) were modeled to predict demolding success. (e-h) Rows of shapes with decreasing  $d/D$  by row. Particularly in (e), the heights are uneven due to inconsistent etching rates.

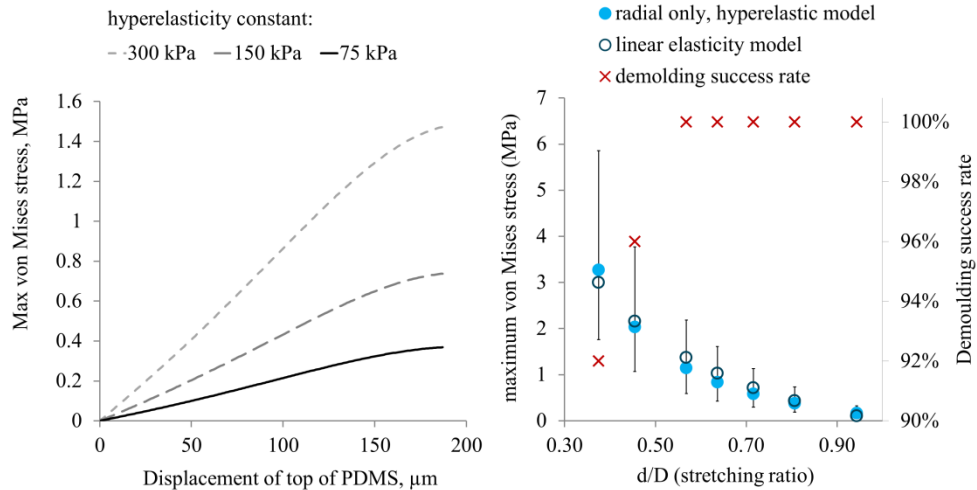


Fig. 4. (Left) The maximum von Mises stress as a function of demolding progress, from the complete model (Fig. 2(b)) for the case  $d/D = 0.64$ , for three different hyperelasticity constants. (Right) The maximum von Mises stress on the PDMS during the linear elastic and hyperelastic model of radial expansion only (Fig. 2(a)) for  $d/D < 1$  (i.e., the cases in which the PDMS stretched around the glass during demolding). Also shown are the experimental rates of successful demolding. For the hyperelastic model, the points represent the model results with the constant C10 at 150 kPa while the error bars represent the effect of changing it from 75 kPa to 300 kPa.

#### Determining demolding success rates

After demolding, some of the PDMS structures showed a lower overall height than originally patterned by the laser, which could have been caused by either a molding failure – some PDMS may have broken off inside the glass mold – or by incomplete etching, meaning that the resulting holes in the mold were not as deep as patterned by the laser. To determine whether broken-off PDMS was still inside the mold, we immersed the glass mold for 2 hours in an aqueous solution of Rhodamine B, which absorbs readily into PDMS [27]. Then, a fluorescence microscope was used to look for bright regions inside the glass, to locate any PDMS remaining in the mold. This technique clearly revealed the presence of PDMS inside the mold in locations where no structures were seen on the molded PDMS (Fig. 5). It was also clear that there was no PDMS located in the regions where the structures were lower than expected, confirming the theory that the decreased height of some structures was from incomplete etching, rather than PDMS breakage.

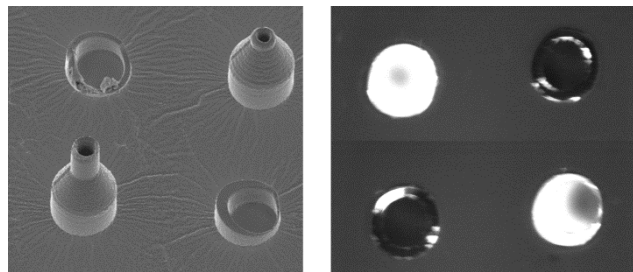


Fig. 5. Identification of demolding success rates is done by comparing the SEM images (left) to images taken of the mold soaked in rhodamine (right); the rhodamine method shows that the top-right shape is incompletely etched in the mold, since there is no rhodamine-infused PDMS broken off in the mold as for the broken samples.



### Comparison of demolding rates and modeled stresses

The modeled shapes had a successful demolding rate of >90% for all ratios of  $d/D$ ; the structures with  $d/D > 0.5$  had 100% success rates of demolding, whereas the  $d/D < 0.5$  structures had a loss of 4-8% of the structures. The failed structures were completely broken off near the plane surface of the PDMS, with nearly all the PDMS remaining inside the glass mold.

While the stress models contain many uncertainties in the PDMS properties and in our demolding process, they qualitatively aligned with our results. They showed a higher total stress on the samples with a smaller  $d/D$  ratio, with the maximum stress in the highest-strain case ( $d/D = 0.38$ ) on the same order as the lowest reported values of the UTS of PDMS. The range of reported material properties of PDMS causes far greater uncertainty than the choice of linear or hyperelastic material models, but for the full range of material properties used, the von Mises stress on the highest-strain case is lower than the range of reported UTS values for PDMS. The more complete model of the  $d/D = 0.64$  case, involving the axial stresses as well as the radial expansion (Fig. 2(a)), yielded maximum von Mises stresses that were within 13% of those found in the hyperelastic radial-expansion-only model, for the same material parameters. This suggests that the forces from the radial expansion are dominant over the axial forces. Given the large uncertainties in the material properties, future models for this application could rely on this simpler radial expansion model for a reasonable first approximation of the demolding stresses.

### Discussion and Conclusions

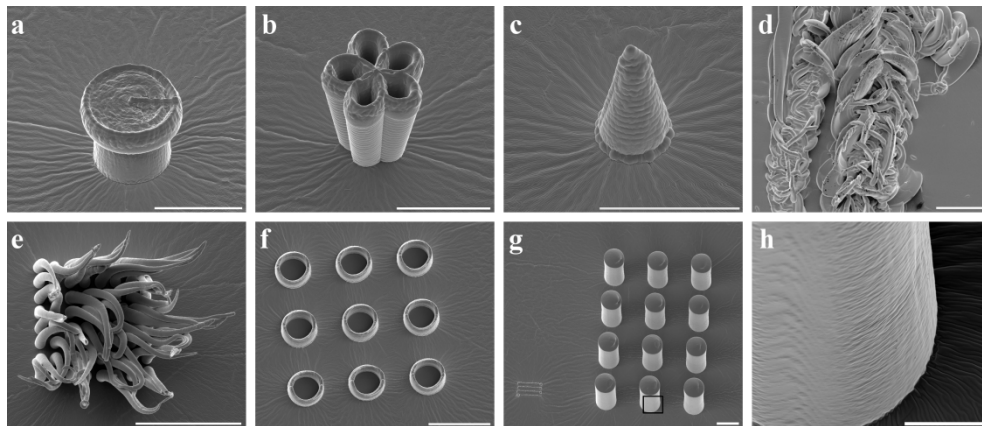


Fig. 6. Examples of PDMS structures fabricated by molding from femtosecond-laser-machined glass substrates. These structures demonstrate the demolding of (a) mushroom-shaped features with significant overhang, (b) thin-walled complex shapes, (c) conical pillars, (d) complex features created by scratching a glass substrate with a diamond-tipped scribe. Highly-repeatable arrays of features (e-h) can also be demolded, including (e) high-aspect ratio pillars, (f) hollow cylinders, and (g) filled cylinders made by molding through-holes in a glass substrate. PDMS demolding allows examination of the machining quality of buried features, which are difficult or impossible to optically image; (h) shows the sidewall quality of the center-bottom pillar in (g). Scale bars for (a)-(g) are 100  $\mu\text{m}$  and for (h), 30  $\mu\text{m}$ .

In addition to the modeled structures, the inverted shape (Fig. 3(b)) and double (vertically-mirrored) versions of the same structures were produced at a variety of aspect ratios (Fig. 3(c and 3d)). We have also produced a wide variety of complex shapes, including some with overhangs or thin walls, as well as highly repeatable arrays of structures with high aspect ratios (Fig. 6). The versatility of the structures which can be made with this technique opens up many potential future applications. Such complex geometries could be employed, for example, to tune surface properties such as wettability and adhesion or to form micro- or

nano-structures functioning as optical devices. It would also be feasible to replicate more rigid materials, by using a two-step molding process with an intermediate PDMS mold. This may be of particular interest for the fabrication of optical components requiring high smoothness, as the secondary molding material could be a thermoplastic; in this case, surface roughness could be decreased by heating to near the transition temperature after demolding.

The final geometry of the structures fabricated with this method depends on several fabrication-process-dependent parameters. The width of the laser-affected zone and the etching rates in the modified and pristine materials affect the wall thickness of the structures formed. Finer control of the laser exposure is possible, and this could be exploited for the fabrication of smaller or thinner-walled structures. For example, the etching rate of the modified region and the surface roughness of the final patterns are highly dependent on the energy deposition conditions and choice of etchant [28–30]. Depending on the size and final application of the structures, process optimization may be required to avoid surface roughness which could adversely affect the demolding process or impact the final application.

The non-linearity of the multiphoton absorption process allows the creation of sub-wavelength features in the glass [31]. In previous work, the fidelity of such structures after demolding was shown to be extremely high, with an average height difference of 1.6 nm between master and mold features [17]. This technique is thus feasible for fabrication on the nanoscale.

In conclusion, femtosecond laser modification and subsequent etching clearly provides a unique method for creating monolithic, mechanically robust molds with complex three-dimensional microfeatures. This technique is made possible by the non-linear laser-material interactions, which allows the formation of arbitrary three-dimensional structures in glass. These structures – including overhangs or complicated geometries – can be replicated with a high success rate due to the high elasticity of PDMS, enabling the fabrication of morphologies which are difficult or impossible to achieve with other microfabrication methods.

### **Acknowledgement**

This work is partially supported by the Femtoprint project (<http://www.femtoprint.eu>), funded by the Factories of the Future initiative (NMP) of the 7th Framework Programme of the European Commission.